HHS Public Access

Author manuscript

Science. Author manuscript; available in PMC 2018 April 20.

Published in final edited form as:

Science. 2017 October 20; 358(6361): 381–386. doi:10.1126/science.aan5468.

D_4 Dopamine Receptor High Resolution Structures Enable the Discovery of Selective Agonists

Sheng Wang[1,$,*], **Daniel Wacker**[1,$,*], **Anat Levit**[2,*], **Tao Che**[1], **Robin M. Betz**[3,4,5,6], **John D. McCorvy**[1], **A. J. Venkatakrishnan**[3,4,5], **Xi-Ping Huang**[1], **Ron O. Dror**[3,4,5,6], **Brian K. Shoichet**[2,$], and **Bryan L. Roth**[1,7,8,$]

[1]Department of Pharmacology, University of North Carolina at Chapel Hill, Chapel Hill, North Carolina, 27599-7365, USA

[2]Department of Pharmaceutical Chemistry, University of California San Francisco, San Francisco, California, 94158-2280, USA

[3]Department of Computer Science, Stanford University, California 94305, USA

[4]Department of Molecular and Cellular Physiology, Stanford University School of Medicine, Stanford, California 94305, USA

[5]Institute for Computational and Mathematical Engineering, Stanford University, Stanford, California 94305, USA

[6]Biophysics Program, Stanford University, Stanford, California 94305, USA

[7]Division of Chemical Biology & Medicinal Chemistry, Eshelman School of Pharmacy, University of North Carolina at Chapel Hill, Chapel Hill, North Carolina 27599-7360, USA

[8]National Institute of Mental Health Psychoactive Drug Screening Program (NIMH PDSP), School of Medicine, University of North Carolina at Chapel Hill, Chapel Hill, North Carolina 27599-7365, USA

Abstract

Dopamine receptors are implicated in the pathogenesis and treatment of nearly every neuropsychiatric disorder. Although thousands of drugs interact with these receptors, our molecular understanding of dopaminergic drug selectivity and design remains clouded. To illuminate dopamine receptor structure, function, and ligand recognition, we determined crystal structures of the D_4 dopamine receptor in its inactive state bound to the antipsychotic drug nemonapride, with resolutions up to 1.95 angstroms. These structures suggest a mechanism for the control of constitutive signaling, and their unusually high resolution enabled a structure-based

[$]Correspondence to: bryan_roth@med.unc.edu(B.L.R.); shoichet@cgl.ucsf.edu(B.K.S.); shengunc@email.unc.edu (S.W.); dwacker@email.unc.edu (D.W.).

[*]These authors contributed equally.

Supplementary Materials
Materials and Methods
Figs. S1 to S15
Tables S1 to S11
References (23–61)
Data set S1

campaign for new agonists of the D_4 dopamine receptor. The ability to efficiently exploit structure for specific probe discovery-rapidly moving from elucidating receptor structure to discovering previously unrecognized, selective agonists-testifies to the power of structure-based approaches.

Dopamine (DA) receptors are G protein-coupled receptors (GPCRs) that are major therapeutic targets for schizophrenia, Parkinson's Disease, drug abuse, and impaired cognition(1). DA receptors are divided into two subfamilies: the $G\alpha_{s/off}$-coupled D_1-like family (e.g. D_1 and D_5 dopamine receptors) and the $G\alpha_{i/o}$-coupled D_2-like family (e.g. D_2, D_3, and D_4 dopamine receptors [DRD2, DRD3 and DRD4])(2). As DRD4 has been implicated in many disorders including attention deficit disorder, metastatic progression and penile erection, DRD4-selective drugs have therapeutic promise(2). Further, although >10,000 drugs and drug-like compounds have been reported to have DA receptor activity (data set S1), our understanding of the molecular mechanisms for DA receptor selectivity and activity is incomplete, as only one relatively low resolution structure--the DRD3--has been reported(3).

To obtain well-ordered crystals for high resolution studies of the human DRD4 in complex with nemonapride, we replaced residues 228–336 of intracellular loop 3 (ICL3) with thermostabilized apocytochrome b562RIL (BRIL) (4) yielding DRD4-BRIL--which has a binding affinity for ^{3}H-N-methylspiperone similar to native DRD4 (Table S2). The DRD4/nemonapride complex crystals diffracted to 1.95 Å resolution (Fig. S1, S2 and Table S1) revealing a full network of water molecules and ions (Fig. 1A). The most dramatic structural differences between the DRD3 (PDB ID: 3PBL) and DRD4 structures are in ECL3, the cytoplasmic ends of TM VI and VII, and the intracellular ends of TM III and V (Fig. S3). Compared to DRD3, TM VI and VII in DRD4 are further apart, with the cytoplasmic tip of TM VI located approximately 2Å closer to TM V (Fig. S3).

The position of DRD3's TM VI appears fixed by an inter-helical hydrogen bond between $Y365^{7.35}$ and $H349^{6.55}$, whereas in DRD4 this is absent as $V430^{7.35}$ cannot hydrogen bond with $H414^{6.55}$ (Fig. S3). Given the critical nature of TMs V and VI in GPCR activation (5), we wondered if this apparent constraint in DRD3 versus DRD4 has functional consequences. A $V430^{7.35}Y$ mutation in DRD4 which recapitulates DRD3's inter-helical hydrogen bond increases DRD4 constitutive activity (Fig. S4A). The reverse mutation in DRD3 ($Y365^{7.35}V$), which mimics DRD4 configuration, diminishes DRD3 constitutive activity (Fig. S4B). Thus, the hydrogen bond between 7.35 and 6.55 potentiates DRD3 constitutive activity, while its absence in DRD4, together with the closer proximity of TM V and VI, may explain the more inactive DRD4/nemonapride structure. Meanwhile, $H^{6.55}$ occupies different rotamer states in DRD4 and DRD3, which could lead to differential ligand binding and activity between the two subtypes, as $H^{6.55}$ forms a direct hydrogen bond with eticlopride in DRD3 (3), while $H^{6.55}$ forms water mediated contacts with nemonapride in DRD4 (Fig. 1, B and C).

High-resolution structures of the A_{2A} adenosine (A_{2A}AR) (Fig. 2A)(6), δ-opioid (δ-OR) (Fig. 2A)(7), β_1-adrenergic (β_1AR)(8), and protease-activated (PAR1)(9) receptors revealed a conserved Na^+/water cluster, coordinated by two highly conserved residues, $D^{2.50}$ and $S^{3.39}$ (10). Here we determined structures of the DRD4/nemonapride complex in the

presence and absence of ~200 mM added sodium and observe an electron density for sodium only when it was added during crystallization (Fig. 2A and S5). This provides the first direct structural evidence for the presence of a sodium ion in its binding site [see (10) for discussion]. Importantly, the DRD4 construct used for crystallization displays similar sodium-dependent allosteric regulation as the wildtype (Fig. S6A). Similar to A_{2A}AR and δ-OR, sodium forms a salt bridge with D80$^{2.50}$ and makes polar interactions with S122$^{3.39}$ and two water molecules in DRD4 (Fig. 2A). A previously described third coordinating water was not observed, likely due to the lower resolution of 2.15 Å (Fig. 2A); the β_1AR 2.1 Å structure also shows weaker density for this water molecule compared to structures of δ-OR and A_{2A}AR (8). Compared with other tested GPCRs, the DRD4 has lower sodium affinity than δ-OR, μ-OR or A_{2A}AR (Fig. 2B–E and S6A–C). As expected (7), lowering [Na+] potentiates DRD4 constitutive activity in a nemonapride-sensitive fashion (Fig. S7).

The sodium pocket in DRD4 adopts nearly identical conformations in the sodium-bound and sodium-free states (rmsd of 0.084 Å, calculated over D80$^{2.50}$, L118$^{3.35}$, S122$^{3.39}$, and four water molecules) (Fig. 2A). Consistent with this finding, MD simulations of the inactive state show that the sodium-free pocket does not collapse even when nemonapride is absent (Fig. S8). Instead, the pocket fills with water and D80$^{2.50}$ and S122$^{3.39}$ become more mobile, though their average positions remain similar to those observed with sodium bound (Fig. S8). MD simulations also predict that sodium's position and mobility is affected by nemonapride (Fig. S9A). With nemonapride bound, sodium mostly occupies a cluster of positions surrounding its crystallographic pose, but occasionally binds a second cluster about 2.5 Å closer to nemonapride, as observed in other GPCRs (11, 12). In simulations of nemonapride-free DRD4, sodium transitioned more frequently between clusters and spent more time in the second cluster, occasionally even occupying the now empty ligand binding site (Fig. S9A, S10 and S11). In both clusters, coordination to D80$^{2.50}$ and S122$^{3.39}$ was largely maintained, with the side-chain hydroxy of S122$^{3.39}$ rotating towards sodium. Interestingly, simulations also indicate that nemonapride's binding pose is more stable in the presence of sodium (Fg. S9B), in agreement with the higher affinity of nemonapride-like ligands in the presence of sodium(13, 14).

Nemonapride interacts with the conserved aspartate D115$^{3.32}$, while it's benzamide ring binds within a conserved orthosteric binding pocket (OBP) lined by residues from TM II, III, V, VI, VII, and ECL2.(Fig. 1, B and C). Nemonapride's conformation is constrained by an intra-molecular hydrogen bond between its amide nitrogen and the methoxy substituent of the benzyl ring. Nemonapride's methoxy ring is fixed by inter-molecular contacts with side chains of the conserved residues F411$^{6.52}$ and V116$^{3.33}$, and by a hydrogen bond with the sidechain of S196$^{5.42}$ (Fig. 1C).

Nemonapride's unsubstituted benzyl group interacts with non-conserved residues V87$^{2.57}$, L90$^{2.60}$, F91$^{2.61}$ and L111$^{3.28}$, all of which have been implicated by mutagenesis for specifying DRD4 pharmacology (15, 16). In the DRD4 structure, these residues emerge as part of a new extended binding pocket (EBP) bordered by TM II and TM III residues (Fig. 1, B and C), distinct from that reported for DRD3 [(3, 17, 18); see Fig. 1D]. This DRD4 EBP: (1) reaches deep into the adjacent position between TM II and TM III (Fig. 1, D and E); and (2) is poorly conserved among the closely related members of the D_2-like subfamily (Fig.

S12). These differences combine to sculpt the distinctive shapes and sizes of the DRD4 and DRD3 EBPs (Fig. 1D), at the core of which is a crevice formed by residues 2.61 and 3.28. In DRD4, nemonapride's unsubstituted benzyl group is wedged between F91$^{2.61}$ and L111$^{3.28}$, indicating that its binding to DRD3 likely requires structural rearrangements to avoid clashes with V86$^{2.61}$ and F106$^{3.28}$ (Fig. 1E).

Docking DRD4-selective ligands against the DRD4/nemonapride structure revealed that their aryl rings docked into the EBP, connecting directly and rigidly to the aminergic heterocycles of the antagonists, unlike nemonapride which is nonselective. As docking forces these rings into contact with specificity residues 2.61 and 3.28 (Fig. S13), we hypothesized that steric clashes with F$^{3.28}$, and lack of interactions with V$^{2.61}$ in DRD3 and DRD2, contribute to DRD4-selectivity. Introducing a F$^{2.61}$V/L$^{3.28}$F double substitution in DRD4 to mimic the DRD2 and DRD3 configuration attenuates affinities of DRD4-selective compounds, with non-selective compounds relatively unaffected (Table S2, S4 and S6). Introduction of the reverse double mutant into DRD2 (V$^{2.61}$F/F$^{3.28}$L) increased the affinity for DRD4-selective ligands without altering the affinities of non-selective compounds (Table S3, S5 and S7), providing an atomic resolution model of DRD4 ligand selectivity (Fig. 1E and S13).

The structural definition of the EBP afforded us the opportunity to seek new DRD4 selective agonists with potentially novel properties, including biased agonism. Accordingly, we docked a library of over 600,000 cationic, "lead-like"(19) molecules from ZINC(20) (http://zinc15.docking.org) against the 1.95 Å DRD4 structure, seeking molecules that bound in both the OBP and EBP (Fig. 3A and METHODS). Of the ten high-ranking molecules tested (Fig. 3B and Table S8) with **3** and **9** being sub-μM agonists with **9** being DRD4 selective (Table S11). Both **3** and **9** are topologically dissimilar to dopaminergic ligands cataloged in ChEMBL20 (21), with the closest dopaminergic analog to **9**, for instance, having a Tc of 0.27, suggesting they represent new dopaminergic scaffolds (Table S11). While **3** and **9** are dissimilar from one another, they share a motif where the central aminergic nitrogen is separated by two carbons from a hydrogen-donating amine which makes a bifurcated hydrogen-bond to Asp115$^{3.32}$ (Fig. 3, C and D).

Seventy-five analogs of **9** were next docked with 15 prioritized for testing based on docking score, EBP occupancy, interaction with Leu187^{ECL2}, and chemical diversity (table S9). All retained the quinolone and aminergic moieties, which engage key residues of the OBP, with most variations in the side chain predicted to interact with EBP residues. For example, **9–6** and **9–11** (Fig. 4A and Table S11) retain the quinolone heterocycle and the bidentate amino groups, with the hydroxymethyl replaced by simple extended side chains to flexibility and deleting a potential competing internal hydrogen bonding group for the aminergic amine. While retaining major interactions of the quinolone heterocycle with the OBP, the increased flexibility of these analogs facilitated better packing against the specificity determining EBP of DRD4 (Fig. 4B and S14A). **9–6** and **9–11** displayed a 20-fold improvement over **9** with no activity at DRD2 or DRD3 at 10 μM (Fig. 4A, 4B, S14A and Table S11). They are potent DRD4 partial agonists (Fig. 4D and S14B) with arrestin bias factors of 20- and 7.8-fold relative to quinpirole (Fig. 4D and S14B). This bias is consistent with the docking, which selected for interactions not only with the EBP but also with predicted arrestin bias-

associated Leu187^{ECL2}(22) with which the conserved quinolone interacts (Fig. 4B and S14A). EBP residue mutations disrupt the affinities of the new agonists (Table S11), consistent with their docked poses (Fig. 4B and S14A).

To improve compound potency and specificity we docked 169 analogs of **9–6** and **9–11** with alternate interactions in the EBP (table S10). We explored many linkers, including those that increased and decreased polarity, flexibility or rigidity, and conservative substitutions off the quinolone ring; ultimately 27 well-fitting, diverse analogs were assayed (Table S10). The most potent were **9-6-23** and **9-6-24** that featured a "right hand side" linker extended to four atoms, the last of being a phenolic ether oxygen. This oxygen, which allows for an internal hydrogen bond to the aminergic amine of the molecule, positions the distal aryl ring over the EBP-defining F91$^{2.61}$ (Fig. 4C)**. 9-6-23** and **9-6-24** had K_i values of 30 and 3 nM at DRD4, respectively, without measurable affinity for either DRD2, DRD3 or the EBP DRD4 mutant F$^{2.61}$V / L$^{3.28}$F, thereby increasing selectivity to >3300-fold (Table S10 and S11). **9-6-24** was a DRD4 partial agonist with a 7.4-fold bias toward arrestin over $G\alpha_{i/o}$ signaling, referenced to quinpirole (Fig. 4E). In counter-screens, neither the parent compound **9-6** nor **9-6-24** had substantial agonist activity against 320 non-olfactory GPCRs (Fig. 4, F and G). The selectivity of **9-6-24** places it among the most potent and specific DRD4 agonists characterized. Meanwhile, **9-6-24**'s arrestin bias contrasts with that of earlier agonists, which are either balanced or slightly G protein biased (Fig. S15). Accordingly, we are making **9-6-24** openly available to the community to use as probe for DRD4 function as **UCSF924** (below).

Here a combination of high resolution structure determination, computational, and biochemical studies has illuminated the structure and function of the DRD4 at atomic resolution. The leveraging of the DRD4 structure for potent and selective ligand discovery—with such discovery occurring contemporaneously with structure determination and functional exploration—attests to the pragmatism of the GPCR structural program for probe and therapeutic lead development.

Supplementary Material

Refer to Web version on PubMed Central for supplementary material.

Acknowledgments

This work was supported by NIH Grants R01MH112205, U19MH82441, HHSN-271-2013-00017-C, and the Michael Hooker Chair for Protein Therapeutics and Translational Proteomics (to B.L.R.) and GM59957 (to BKS). We thank J. Sondek and S. Endo-Streeter for independent structure quality control analysis; M. J. Miley and the UNC macro-molecular crystallization core for advice and use of their equipment (P30CA016086); James W. Murphy for running FRAP assays; B.E. Krumm for advice on data processing; J. Smith, R. Fischetti and the staff of GM/CA@APS, supported by the US NCI (ACB-12002) and the US NIGMS (AGM-12006). This research used resources of the Advanced Photon Source, a U.S. Department of Energy (DOE) Office of Science User Facility operated for the DOE Office of Science by Argonne National Laboratory under Contract No. DE-AC02-06CH11357. Coordinates for the two structures 5WIU and 5WIV are available at the Protein Data Bank (numbers to be made available after manuscript acceptance). UCSF924 is available as a molecular probe via Sigma Millipore (SML2022 and SML2023 for the active and deactivated agonists, respectively)

References and Notes

1. Missale C, Nash SR, Robinson SW, Jaber M, Caron MG. Physiol Rev. 1998; 78:189–225. [PubMed: 9457173]
2. Beaulieu JM, Espinoza S, Gainetdinov RR. Br J Pharmacol. 2015; 172:1–23. [PubMed: 25671228]
3. Chien EY, et al. Science. 2010; 330:1091–1095. [PubMed: 21097933]
4. Chu R, et al. J Mol Biol. 2002; 323:253–262. [PubMed: 12381319]
5. Rasmussen SG, et al. Nature. 2011; 477:549–555. [PubMed: 21772288]
6. Liu W, et al. Science. 2012; 337:232–236. [PubMed: 22798613]
7. Fenalti G, et al. Nature. 2014; 506:191–196. [PubMed: 24413399]
8. Miller-Gallacher JL, et al. PLoS One. 2014; 9:e92727. [PubMed: 24663151]
9. Zhang C, et al. Nature. 2012; 492:387–392. [PubMed: 23222541]
10. Katritch V, et al. Trends Biochem Sci. 2014; 39:233–244. [PubMed: 24767681]
11. Gutierrez-de-Teran H, et al. Structure. 2013; 21:2175–2185. [PubMed: 24210756]
12. Vickery ON, Machtens JP, Tamburrino G, Seeliger D, Zachariae U. Structure. 2016
13. Neve KA. Mol Pharmacol. 1991; 39:570–578. [PubMed: 2017157]
14. Michino M, Free RB, Doyle TB, Sibley DR, Shi L. Chem Commun (Camb). 2015; 51:8618–8621. [PubMed: 25896577]
15. Simpson MM, et al. Mol Pharmacol. 1999; 56:1116–1126. [PubMed: 10570038]
16. Schetz JA, Benjamin PS, Sibley DR. Mol Pharmacol. 2000; 57:144–152. [PubMed: 10617689]
17. Newman AH, et al. J Med Chem. 2012; 55:6689–6699. [PubMed: 22632094]
18. Michino M, et al. Mol Pharmacol. 2013; 84:854–864. [PubMed: 24061855]
19. Oprea TI, Davis AM, Teague SJ, Leeson PD. J Chem Inform Comp Sci. 2001; 41:1308–1315.
20. Sterling T, Irwin JJ. J Chem Inf Model. 2015; 55:2324–2337. [PubMed: 26479676]
21. Bento AP, et al. Nucleic Acids Res. 2014; 42:D1083–1090. [PubMed: 24214965]
22. Wacker D, et al. Cell. 2017; 168:377–389. e312. [PubMed: 28129538]

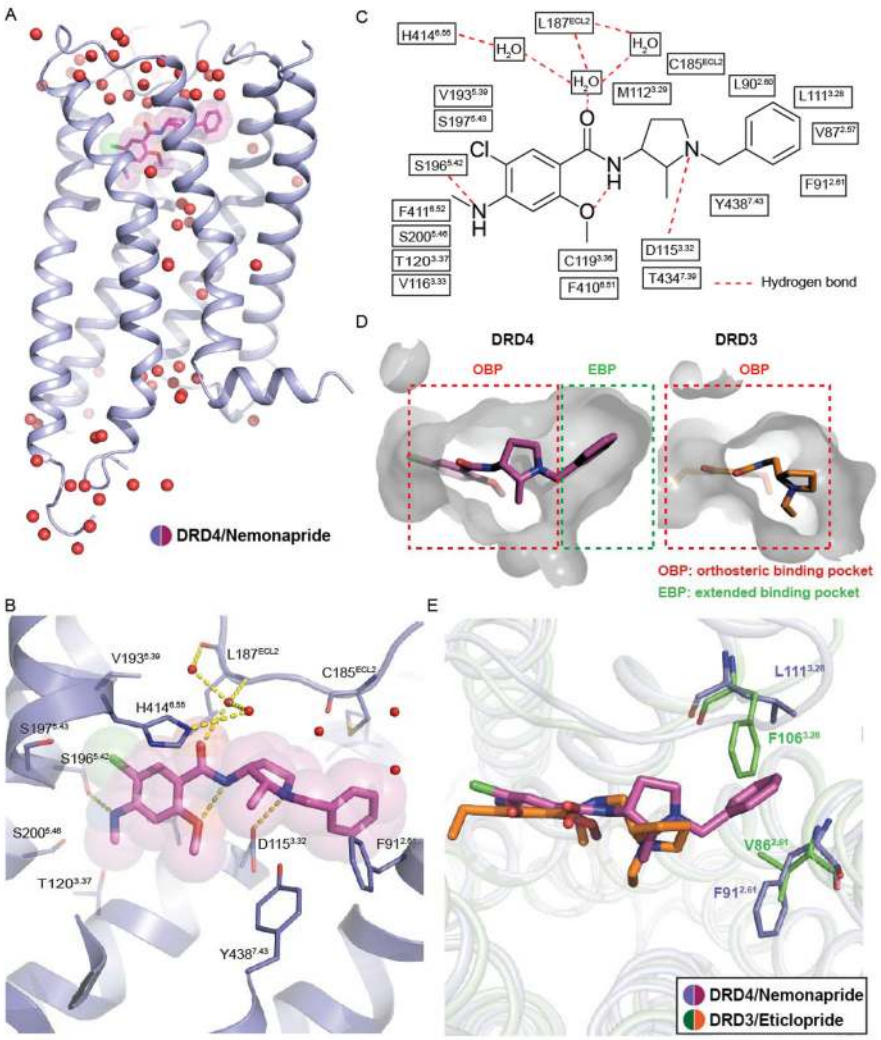

Fig. 1. Human D4 –nemonapride complex

A, Overview of the DRD4-nemonapride complex structure with water molecules depicted as red spheres. **B**, Conformation of the binding pocket with nemonapride shown by sticks with magenta carbons. The protein is displayed in cartoon representation, with the 11 contact residues within 4.0 Å from the ligand shown by slate blue sticks. Structured water molecules are shown as red spheres. Ballesteros–Weinstein numbering is shown as superscript. **C**, Diagram of ligand interactions in the binding pocket side chains at 4.0 Å cut-off. Hydrogen bonds are shown in dashed lines. **D**, Side views of the sliced binding pocket in DRD4-nemonapride and DRD3-eticlopride complex. The pocket surfaces are colored gray. Ligands are shown as capped sticks with carbons colored magenta (Nemonapride) and orange (eticlopride). **E**, the different position of phenylalanine in DRD4 (slate blue) and DRD3 (green). Ligands are colored as in panel **D**.

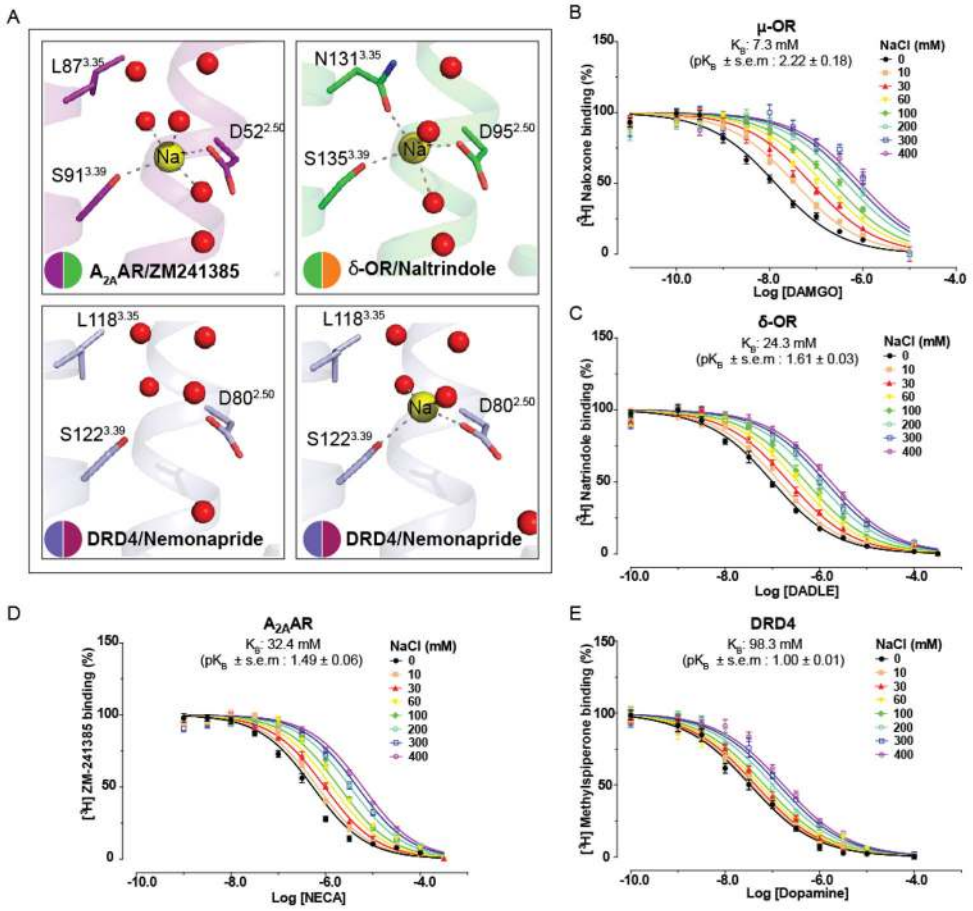

Fig. 2. Structural and functional details of the DRD4's allosteric Na^+ site

A, Close ups of A_{2A} adenosine receptor (magenta), δ-OR receptor (green), D4 dopamine receptor without sodium (slate blue) and D4 dopamine receptor with sodium (slate blue) respective Na^+ allosteric pockets are shown as inserts. The receptors are shown as a ribbon, and residues lining the Na^+ cavity are shown as sticks and labeled according to Ballesteros-Weinstein scheme. Water molecules in the cluster are shown as red spheres. Na^+ is displayed as yellow spheres. The salt bridge between Na^+ and $D^{2.50}$ and hydrogen bonds are shown as grey dotted lines. **B, C, D, E,** The allosteric effect of graded dose of sodium on DAMGO, DADLE, NECA or dopamine affinity were respectively measured at μ-OR (**B**), δ-OR (**C**), A_{2A}AR (**D**) and DRD4 (**E**).

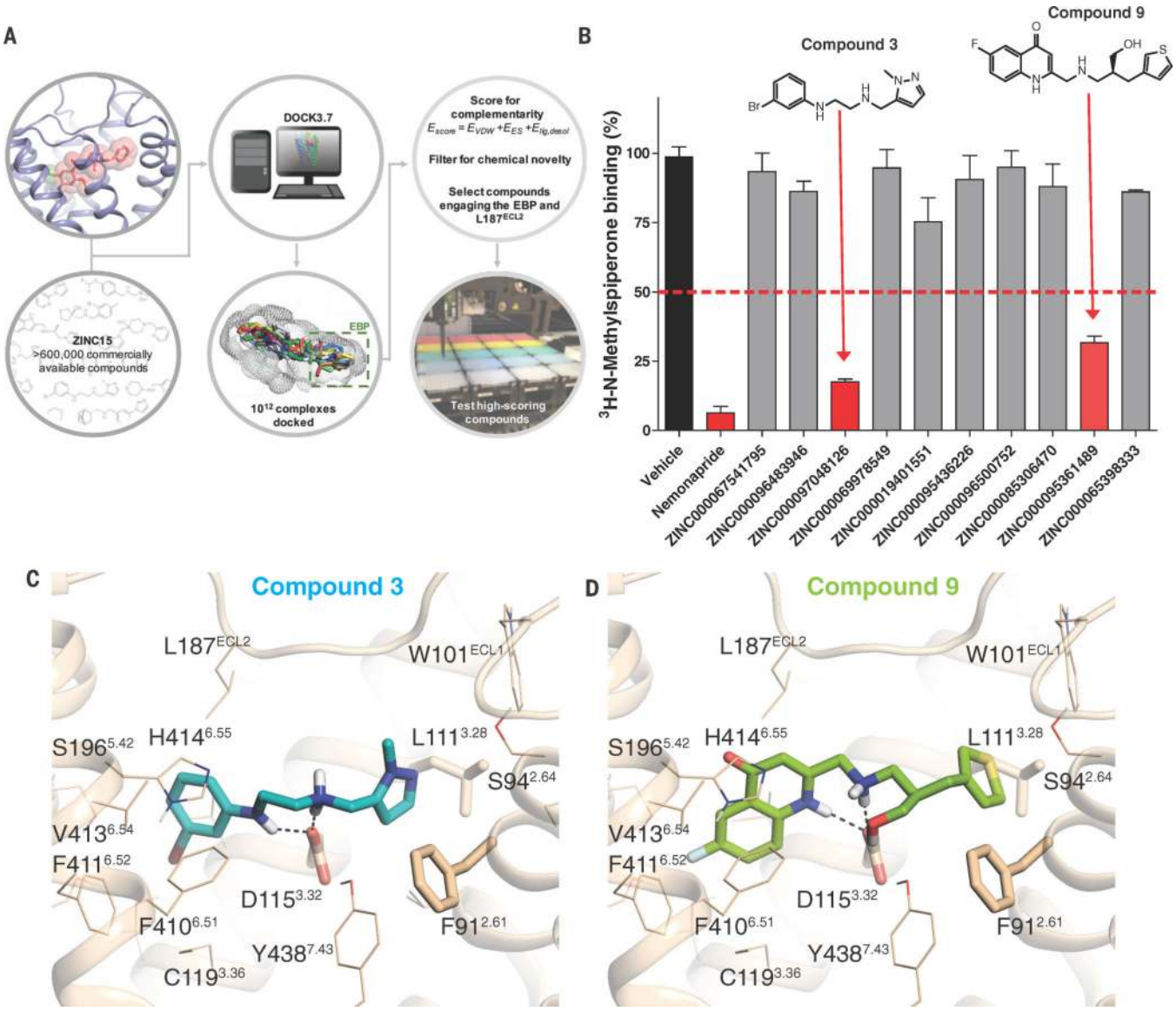

Fig. 3. Discovery of a new DRD4 selective agonist

A, Structure-based strategy for discovery of novel DRD4 chemotypes from docking screens against large virtual libraries. **B**, Single-point competition binding assay of 10 candidate molecules against the DRD4 antagonist ^{3}H-N-Methylspiperone. Each ligand was tested at 5 μM and for those with > 50% inhibition affinity was calculated in full displacement curves; data represent mean ± s.e.m. (n = 3 measurements). **C**, D Docking poses of compounds 3 (**C**) and 9 (**D**), new DRD4 agonists. The D_4 dopamine receptor and residues are shown in tan. Compounds are shown as capped sticks with carbons colored cyan (compound **3**) and green (compound **9**). Ballesteros–Weinstein numbering is shown as superscript.

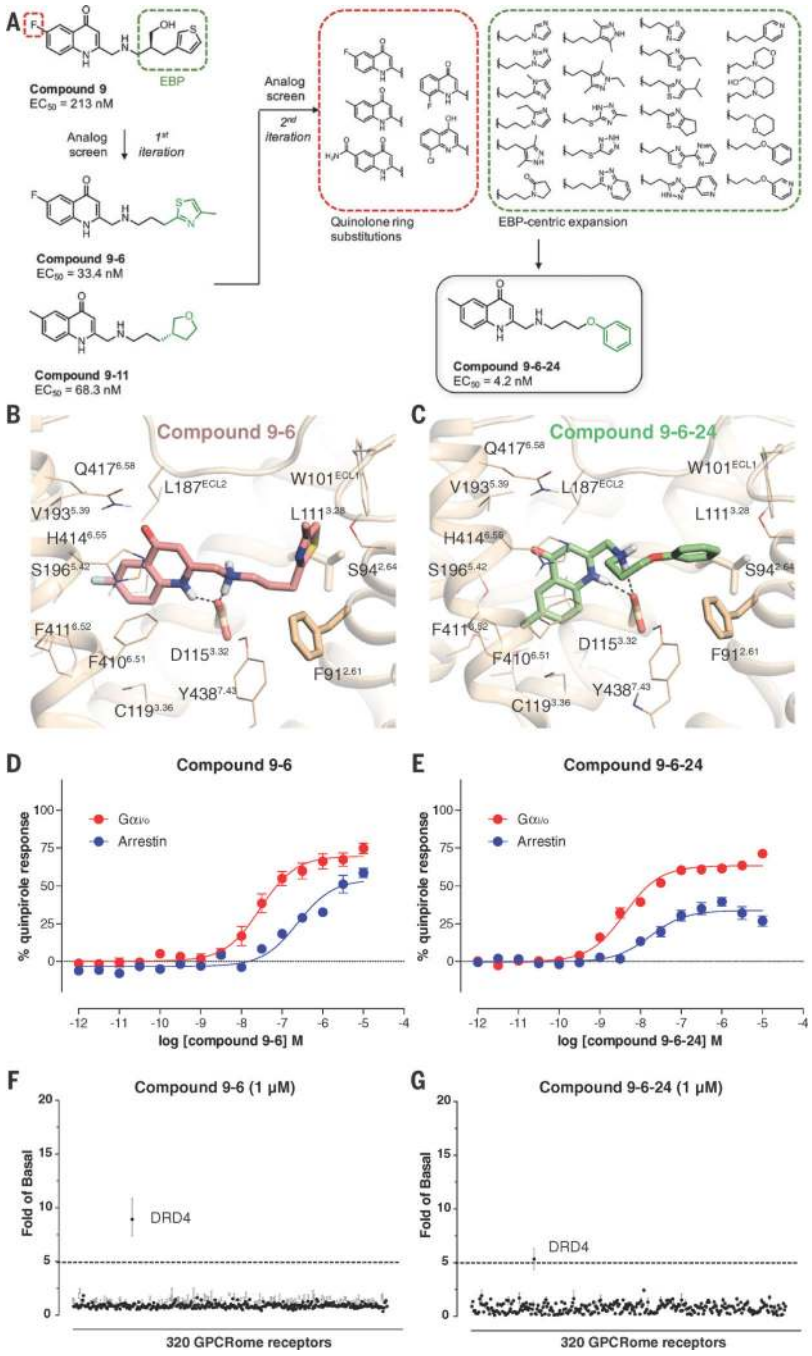

Fig. 4. Structure-guided optimization of potent DRD4 agonists

A, Overview of structure-guided analog-by-catalog optimization towards compound **9-6-24** (see main text for details). **B, C,** Docking poses of compounds **9-6** (**B**) and **9-6-24** (**C**). Both optimized analogs have a simplified right hand linker while maintaining key interactions and occupying the EBP. The D4 dopamine receptor and residues are shown in tan. Compounds are shown as capped sticks with carbons colored pink (compound **9-6**) and green (compound **9-6-24**). Ballesteros–Weinstein numbering is shown as superscript. **D, E,** Normalized concentration-response studies for compound **9-6** (**D**) and **9-6-24** (**E**) at human cloned

DRD4–mediated activation of $G\alpha_{i/o}$ and arrestin translocation. Error bars in (**D**) and (**E**) denote SEM from a minimum of three assays. See METHODS for details on bias factor calculation. **F, G,** Compound **9-6** (**F**) and Compound **9-6-24** (**G**) were screened against 320 non-olfactory GPCRs for agonism in the arrestin recruitment TANGO assay. Each point shows luminescence normalized to basal level at a given GPCR, with vertical lines indicating the standard error of the mean.